Temperature memory effect of stress annealing-induced anisotropy in metallic glasses

Pawel Kozikowski,[1,*] Masato Ohnuma,[1,†] Ryuichi Hashimoto,[1]
Kodai Takano,[1] Giselher Herzer,[2] Markus Kuhnt,[2,‡] and Christian Polak[2]
[1]*Division of Quantum Beam Science, Hokkaido University, Kita 13 Nishi 8, Kita-ku, Sapporo 060-8628, Japan*
[2]*Vacuumschmelze GmbH & Co. KG, D-63450 Hanau, Germany*

(Received 5 August 2020; accepted 8 September 2020; published 25 September 2020)

Stress annealing (SA)-induced magnetic anisotropy is known in iron, nickel, and cobalt-based ferromagnetic metallic glass ribbons and it has already been used in commercial processes. Uniaxial elastic strain is introduced by SA and is quenched into the ribbons even after cooling and removing the external stress. The release of the uniaxial quenched strains is clearly observed as an anomaly in the linear thermal-expansion coefficient (LTEC) when the ribbon is reheated without stress. The rate of strain release corresponding to the LTEC anomaly reaches a maximum at the temperature at which the original SA was performed. We have observed this temperature memory effect over the whole temperature range from 280 to 400 °C, which is below the crystallization temperature T_x. The observed results are explained well by the existence of a localized "flow unit" embedded in an elastic matrix, which is accepted as the origin of the shear band formation and rejuvenation of metallic glasses with T_g (glass transition temperature) $<T_x$. Although T_g is hardly visible in calorimetry measurements in most of the ferromagnetic metallic glass ribbons ($T_g > T_x$), the results here indicate that the same important structural feature is common to metallic glasses with both $T_g < T_x$ and $T_g > T_x$. Because magnetization behavior is very sensitive to the existence of residual elastic strain which is difficult to evaluate in most of the metallic glasses, detailed studies and a revival of interest in ferromagnetic ribbons will help us to understand more about the nature of the localized flow unit, as well as nonaffine deformations.

DOI: 10.1103/PhysRevMaterials.4.095604

I. INTRODUCTION

Iron, nickel, and cobalt-based amorphous ribbons are the most successful commercial metallic glass systems ever discovered. They are used as soft ferromagnetic materials, from antitheft devices to power transformers because of low core loss and/or their controllable magnetic anisotropy [1–5]. Except for some multicomponent systems [6], the glass transition temperature T_g for most of those ferromagnetic metallic glass ribbons does not appear below the crystallization temperature T_x in regular calorimetric measurements, and it is not possible to form "bulk" shapes using them. As a result, they have received less attention in the latest structural studies of metallic glasses, which are mostly of bulk glass forms with $T_g < T_x$.

Apart from the ideal homogeneous random structure of glassy materials themselves, the spatial heterogeneity of mechanical response, such as the elastic constant, thermal expansion, and/or relaxation have attracted recent interest due to the relation to mechanical ductility [7–15]. Formation of a shear band where the localization of flow occurs is related to the heterogeneity of the elastic modulus [7,8]. In a rejuvenation process, a nonaffine deformation due to the heterogeneity causes thermal strain by cyclic cooling. Since the induced strain is isotropic, the resulting change in structure is regarded as an increase of free volume which modifies the ductility of metallic glasses [14,15]. The existence of a localized "flow unit" (called also a "liquidlike zone" [11], "loosely packed region" [15], or "weakly bonded region" [16]) surrounded by an elastic matrix is proposed as the source of nonaffine deformation which is the key structural change involved in the formation of a shear band [8–12] and rejuvenation [13–15]. Thermal analysis [10–13] and simulations [12,15,17] as well as acceleration of crystallization by ultrasonic vibration [16] show that the flow unit has the feature of β relaxation, which has a lower relaxation temperature and lower activation energy than α relaxation including glass transition [10,11].

Such a nonaffine deformation may cause residual strain after deformation. Tong *et al.* showed the existence of elastic strain induced by severe plastic deformation of bulk metallic glasses [18]. No other work has been reported due to the difficulty of evaluation of residual strain in a glassy single phase. Consequently, the effect of residual strain is thought to be small and is usually ignored [11]. Contrary to the metallic glasses with $T_g < T_x$, which are mostly nonmagnetic, the existence of residual strain has been widely accepted in ferromagnetic metallic glass ribbons since the 1970s [19,20]. Since the magnetization process and coercivity H_c is very sensitive to the strain due to the magnetoelastic effect, the existence of quenched strain in as-quenched ribbons was deduced from the change of H_c by annealing at a moderate temperature lower than T_x [19–21].

*Present address: Central Institute for Labour Protection National Research Institute, ul. Czerniakowska 16, 00-701 Warsaw, Poland.
†Corresponding author: ohnuma.masato@eng.hokudai.ac.jp
‡Present address: Institut Dr. Foerster GmbH & Co. KG, In Laisen 65, 72766 Reutlingen, Germany.

The sensitivity of magnetization behavior on residual strain was also probed by the change of H_c through cold rolling, followed by annealing [22]. In contrast to the magnitude of H_c related to multidirectional strain (or stress) in the as-prepared and cold rolled ribbons, the uniaxial anisotropy of the magnetization curve was observed under applied stress due to the magnetoelastic effect [23]. Although the effect is reversible after removing the external stress, the permanent effects appear when the ribbon is annealed under the stress [from here, this is called stress annealing (SA)] [23–25]. The quantitative analysis of uniaxial anisotropy energy K_u (or anisotropy field H_k) induced by different temperatures and stresses of SA has been studied [26,27]. By combining it with a flash annealing technique [28,29], SA becomes commercially important for tailoring uniaxial anisotropy depending on the application purpose [4,5]. The structural origin of SA-induced magnetic anisotropy of $Fe_{81}B_{13}Si_4C_2$ has been reported using synchrotron radiation as resulting from the residual bond anisotropy after removing the external stress [30]. The SA-induced magnetic anisotropy has also been recovered by postannealing [26]. A corresponding structure recovery has been reported in $Fe_{40}Ni_{40}B_{20}$ metallic glass ribbons by linear thermal-expansion (LTE) measurements [31]. From the relation between structural anisotropy and their recovery measured by x-ray diffraction and LTE for ferromagnetic metallic glass ribbons with nine different compositions [32,33], the existence of residual strain caused by SA has been concluded. One of the unique features found during recovery of SA-induced structural anisotropy is that the temperatures where the maximum rate of strain release occurs during postannealing are independent of their compositions, while the magnitudes of induced structural and magnetic anisotropy do strongly depend on them [33].

In this paper, we applied the same technique as in previous work [32,33] to a $Co_{72.5}Fe_{1.5}Mn_4Si_5B_{17}$ amorphous ribbon annealed at different temperatures under tensile stress and found that they memorize the temperatures of SA. The phenomena are explained well by the existence of a localized flow unit (β-relaxation region) that has recently been proposed as the dominant structural motif operating in metallic glasses to explain shear band formation and rejuvenation.

II. EXPERIMENTAL METHODS

$Co_{72.5}Fe_{1.5}Mn_4Si_5B_{17}$ metallic glass ribbons with a width of 6 mm and a thickness of 21 μm were made by a rapid-quenching technique in air. SA was performed using a continuous annealing system where amorphous ribbons are fed into the 1-m-long furnace continuously under tensile stress. SA experiments were performed two times with two different atmospheres, one in air and the other under N_2 flow. Details of the continuous annealing system are given in [34]. The ribbons were annealed for 30 sec at different annealing temperatures ranging from 280 to 400 °C. All of those temperatures are below $T_x = 480$ °C measured with a heating rate of 20 K/min. The stress was applied by a weight which corresponds to 320 MPa for the ribbons before SA and to 360 MPa for the ribbon after SA. The difference is caused by permanent elongation (3–5%) along the tensile stress direction and thinning of the ribbons during the process. The induced magnetic anisotropy energy K_u at a SA temperature of 350 °C is 21 J/m^3.

XRD profiles were measured in transmission mode to locate the scattering vector q in the ribbon plane. To achieve a high transmission rate, the Mo-$K\alpha$ line ($\lambda = 0.070\,93$ nm) was used together with an incident monochromator and a solid-state detector (Rigaku ultraX system). Two measurements were conducted for each sample: one for the measurement with the vector **q** parallel to the tensile stress direction (ribbon length direction), and the other with the vector **q** perpendicular to the tensile stress direction (ribbon width direction). From the two scattering profiles, the two halo top positions were determined as $q_{p\|}$ (scattering vector **q** parallel to tensile stress) and q_{p+} (perpendicular to tensile stress). Here, the magnitude of **q** is determined as follows:

$$q = |\mathrm{q}| = 4\pi \sin\theta/\lambda \quad (2\theta : \text{scattering angle}).$$

For the case of crystalline materials, the elastic strain $e_{\|}$,e_+ can be evaluated using the peak position at a stress-free condition, q_0, as follows;

$$e_{\|} = (q_0 - q_{p\|})/q_{p\|}, \quad e_+ = (q_0 - q_{p+})/q_{p+}.$$

However, for amorphous materials, the above equation cannot be used directly due to the lack of periodicity of atomic planes. Thus, as with the previous Refs. [31,32], we introduce the anisotropy parameter Δq as the simple form

$$\Delta q = q_{p+} - q_{p\|}.$$

Thermomechanical analysis (TMA) was employed to measure the linear thermal expansion (LTE) and its coefficient (LTEC) of the SA ribbons. The measurements were performed using a Rigaku TMA (Thermo plus 2) with different heating rates ranging from 5 to 50 K/min under an N_2 flow. A ribbon with the length of about 14 mm was gripped by the holder and the length change of a 10-mm portion between the holder arms was measured. After shrinkage by stress release, slipping at the grip sometimes occurred which appeared as a dip in the TMA curve, thus making it easy to find such occurrences. In order to minimize the experimental uncertainty related to these dips, we evaluated only experiments with no such dips or only minor pronounced dips as was the case with the 320 °C curve.

III. RESULTS

Figure 1(a) shows LTE measured with a heating rate of 20 K/min for the ribbons annealed at different SA temperatures. All ribbons show clear shrinking at about 480 °C corresponding to T_x. In addition, all the ribbons show an anomaly at the temperatures marked by arrows. By taking the temperature derivative, the linear thermal-expansion coefficient (LTEC) can be evaluated from the LTE curves and they are plotted in Fig. 1(b). Although there is some scatter in the absolute values of LTEC, due to the difficulty of gripping the ribbons, all show a clear anomaly in LTEC, indicating that anomalous shrinking occurs during this annealing process for LTE measurements. The measured LTEC is along the direction of tensile stress during annealing; the results indicate that the elastic elongation introduced by SA is released by the second annealing for LTE measurements. It also shows a unique

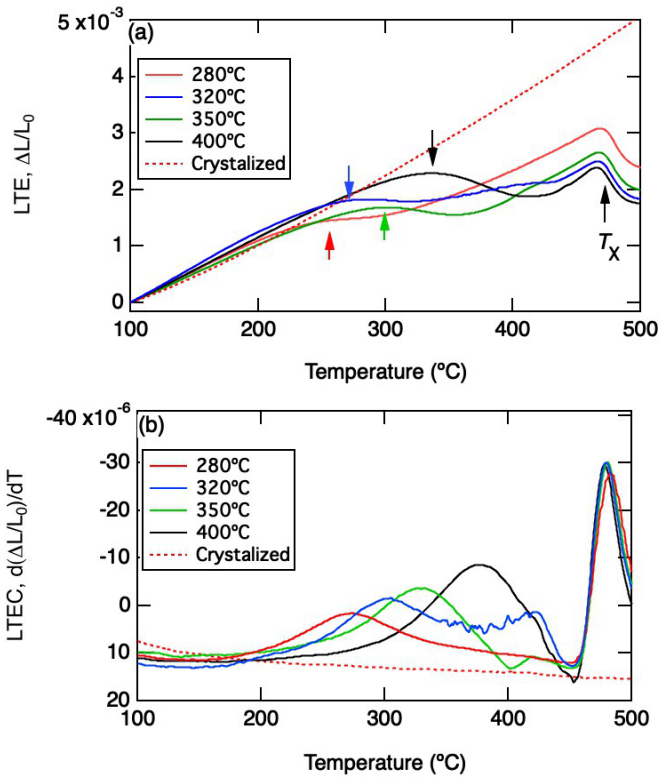

FIG. 1. (a) Linear thermal expansion (LTE) and (b) LTE coefficient (LTEC) for the different SA temperatures. Arrows in (a) indicate the starting point of the anomaly corresponding to shrinking in the ribbon direction (= tensile stress direction of SA).

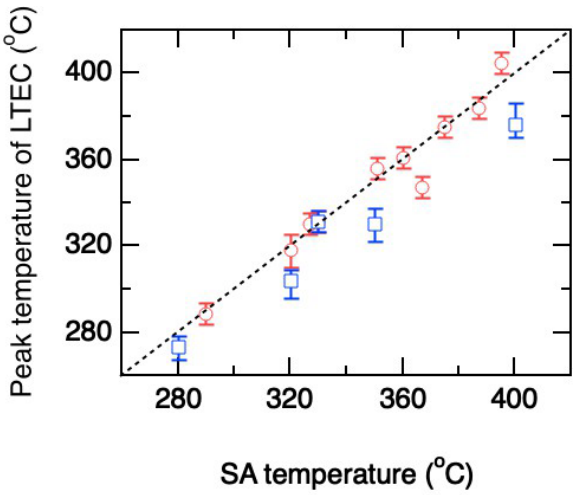

FIG. 2. Relation between SA temperatures and peak temperatures in LTEC. The difference in colors correspond to two experiments with different atmosphere (blue: in air; red: under N_2 flow). The dotted line corresponds to the case that peak temperature perfectly agree with the SA temperature.

feature that the maximum rate of strain release, corresponding to the peak of the LTEC curves, occurs at about the same temperatures used for the SA. The results suggest that the ribbons memorize the SA temperature, which we call a "temperature memory effect." To confirm this, more SA temperatures in the range from 280 to 400 °C were tested. Though there are some differences depending on the differences between the sets of continuous annealing experiments, the temperature memory effect is clearly observed at all of our observed temperatures, as shown in Fig. 2. Note that the effect can appear in the wider temperature range below T_x.

The level of SA induced strain has also been evaluated by the transmission x-ray diffraction (XRD) technique. The halo peak positions are different depending on the measured scattering vector parallel and perpendicular to the tensile stress as shown in Fig. 3, indicating that some elongation occurs parallel to the external stress during SA. The amount of quenched elastic strain is also calculated from the total area of the peak shown in Fig. 1(b). The ribbons with lower SA temperatures show some shoulders, corresponding to the remaining strains induced during the melt-quench process. Those strains below the SA temperature had already been released during SA, while the strains that required a higher temperature for release remained and exhibited a shoulder in the higher temperature range than that of the peak [33]. To suppress their effects in the evaluation of SA induced strain, the integral was taken up to 50 °C higher than the peak. The values are shown in Fig. 4 together with the anisotropy parameter Δq (the definition of Δq is given in Sec. II) determined from XRD measurements. The results indicate that even for the same external tensile stress applied during SA, the amount of quenched strain increased by increasing the SA temperatures. The maximum quenched strain reaches 0.25% (0.0025 as a fraction) which is about 1/20 smaller than the permanent elongation, about 3–5%. If we apply the equation for the strain evaluation for crystalline materials (see Sec. II), the maximum Δq yields a value of about 0.2% which agrees well with the value determined by LTE measurements.

To further clarify the features of stress release, activation energies were evaluated by the peak position of LTEC for different heating rates using the simple Kissinger equation

$$\ln\left(A/T_p^2\right) = B - W^*/(RT). \quad (1)$$

Here, A is the heating rate of the LTE measurements, T_p is the temperature of the peak in Fig, 1(b), B is a constant, and R is the gas constant. The activation energy of stress release, W^*, for different SA temperatures corresponds to the gradient of the lines in Fig. 5. The value of W^* for SA at 280 °C yields 101 kJ/mol and increases up to 187 kJ/mol at 400 °C, while the activation energies of T_x are 294 kJ/mol, and are of course identical for the ribbons with different SA temperatures. Similar variations of activation energies for the recovery of SA-induced structural anisotropy have been reported for $Fe_{40}Ni_{40}B_{20}$ ribbons annealed under different SA temperatures [31].

IV. DISCUSSION

The features of temperature memory effects of strain release we observed can be explained by the existence of a localized flow unit (localized β relaxation region) surrounded by an elastic matrix, as has been proposed by previous studies [8,10,11,35], and is illustrated in Fig. 6(a). The dotted green curve shows the original (before SA) shape of the "cage" which is formed by the innermost atoms in the elastic matrix.

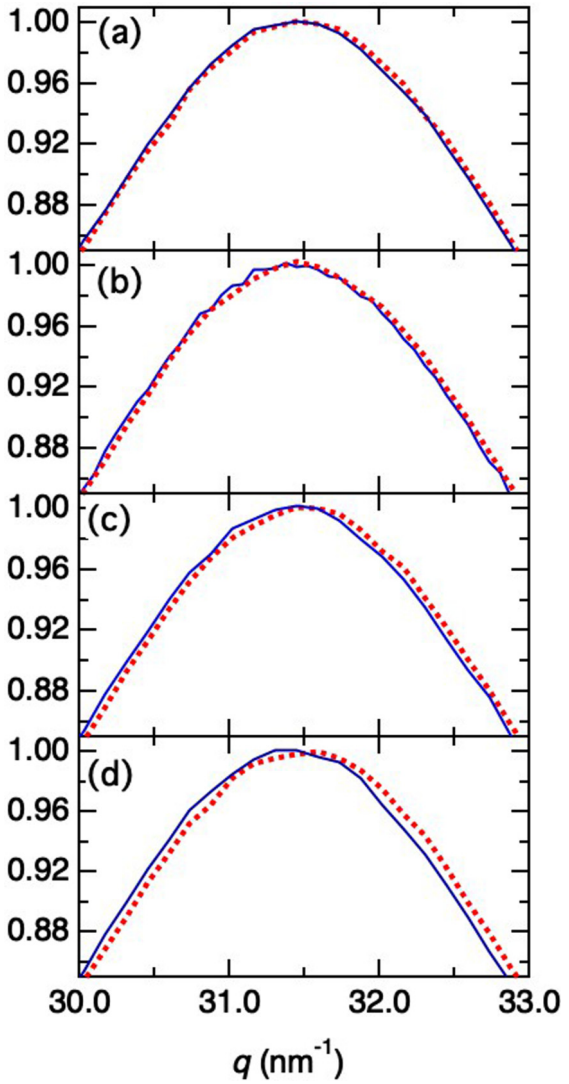

FIG. 3. The transmission XRD profiles around the halo top position for the SA temperatures of (a) 280 °C, (b) 320 °C, (c) 350 °C, and (d) 400 °C. Solid and dotted curves correspond to the profiles measure with q parallel and perpendicular to the tensile stress direction of SA, respectively.

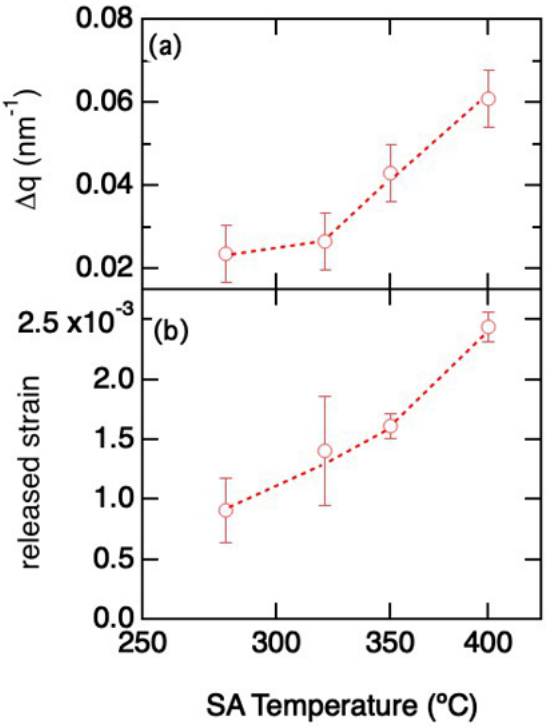

FIG. 4. The degree of structural anisotropy determined by transmission XRD and amount of release strain determined as the area of the peak in the LTEC. The integrals are calculated up to 50° above the peak temperatures.

When the stress is applied at room temperature, both flow unit (atoms in red color) and elastic matrix (atoms in blue color) deform elastically [Fig. 6(b)]. The shape of the cage also changes elastically as shown by the solid green curves. The distance from atoms 3 to the line between and atoms 1 and 2 (called "line 1-2" from here) which is perpendicular to the tensile stress, expands elastically. If the external stress is released under this condition, the distance between 3 and line 1-2 as well as the shape of the cage revert back to the original as shown in Fig. 6(a). However, in SA, the mobility of atoms in the cage is high enough, due to their loosely packed state, that they will slowly change the positions to release local elastic energy and slowly accommodate to the shape of the elongated cage [solid green curves and the position changes of red atoms in Fig. 6(c)]. On removing the external stress at this elevated temperature, the atoms in the cage can rearrange again to the original shown in Fig. 6(a) because they can accommodate again to the original cage shape shown by the dotted green curve. However, in the case that the external stress is removed after cooling down to room temperature which is the condition of SA, the cage shape cannot revert back to the original dotted (stress-free) form due to the frozen atomic arrangement inside the flow unit [Fig. 6(d)]. Consequently, some part of the elastic elongation in the elastic matrix remains as quenched strain even after removing the external stress, which is schematically expressed as the distance between 3 and line 1-2 in Fig. 6(d). Since the stable shape of the cage without the external stress is the dotted line, the atoms inside the cage accommodate

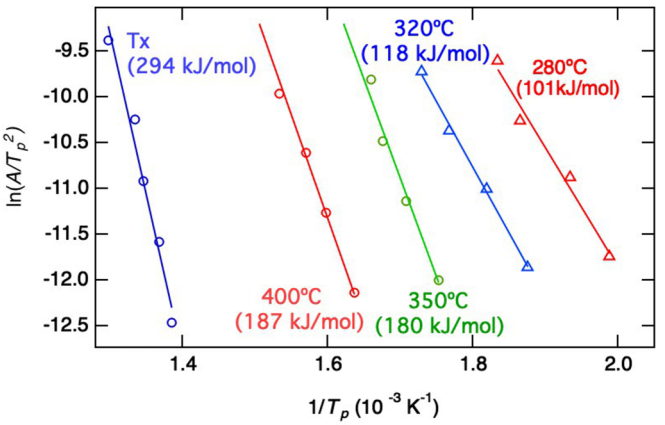

FIG. 5. Kissinger plots of the peak position in LTEC for the ribbons treated at different SA temperatures.

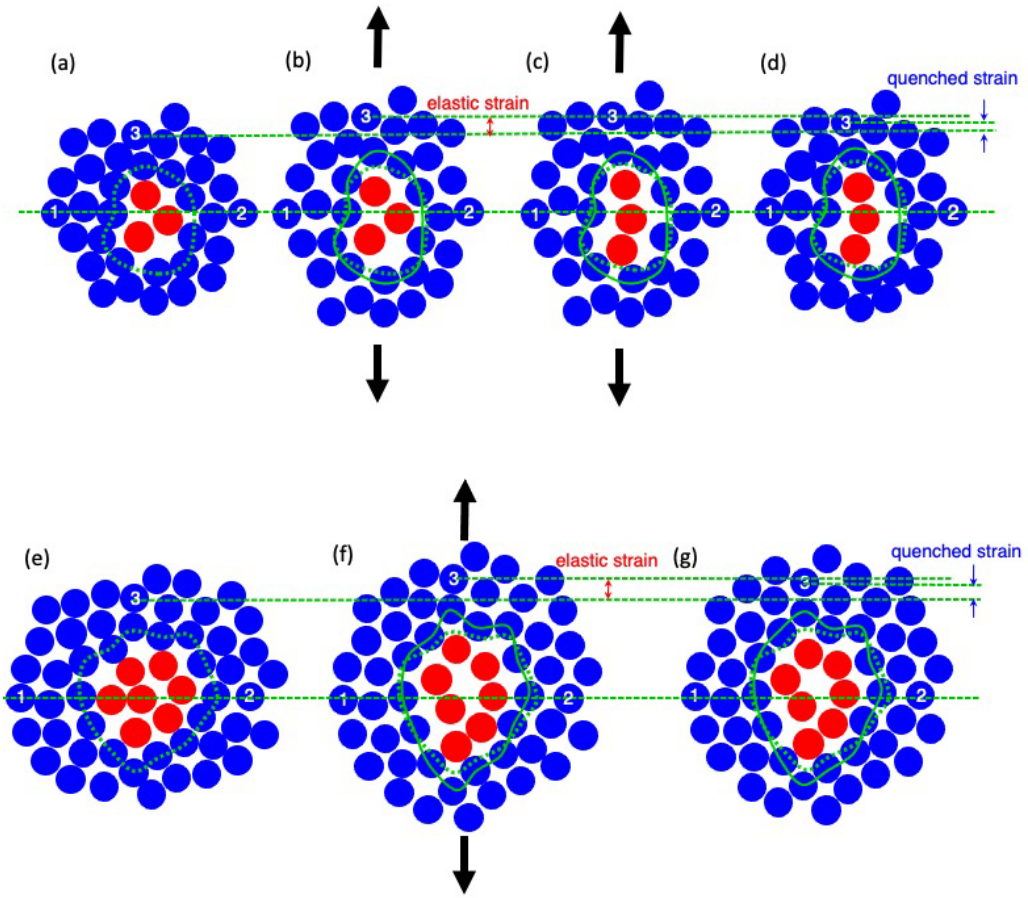

FIG. 6. Models for the mechanism of the temperature memory effect. Panels (a)–(d) correspond to the lower SA temperatures at which the small size of flow unit is the source of the temperature memory effect. Panels (e)–(g) show that the larger flow unit corresponds to the source of temperature memory effects at higher SA temperatures. In (a)–(g), atoms inside the flow unit are shown in red and atoms in the elastic matrix are shown in blue. Dashed green lines are eye guides for the elastic strain, i.e., the distance between 3 atoms and the line 1-2 is perpendicular to the external stress. The atoms in blue can move only elastically through the SA, while the atoms in red have high mobility when ribbons are heated for SA. The dotted green curves show the original (before SA) shape of a cage formed by the innermost atoms in the elastic matrix. The solid curve shows the elastically deformed cage produced by the external stress (b), (c), (f) or the accommodation of atoms inside the cage (d), (g).

when the ribbons are reheated for LTE measurements and the shrinking of ribbons occurs.

The key for the appearance of the temperature memory effect is the fact that the number density of atoms inside the cage changes little through SA to reheating for LTEC measurements. Based on the model for potential energy barrier of a shear transformation zone [36,37], Liu *et al.* [10] have proposed the following equation to correlate the activation energy and the flow unit volume:

$$\Omega = W^*/(8/\pi^2)\gamma_c^2 \xi G. \tag{2}$$

Here, Ω is the volume of the flow unit, γ_c is the critical shear strain, ξ is a correction factor arising from the matrix confinement of a flow unit, and G is the shear modulus. Because the ribbon is still 100% amorphous phase, γ_c and G are basically the same before and after SA. If the same volume of the flow unit is maintained through the process, the activation energy W^* keeps the same value before and after SA, which means atoms inside the flow unit become mobile at about the same temperature before and after SA. Consequently, the temperature for the release of strain appears at about the same temperature as used for the SA.

The dependence of the total amount of quenched strain on the SA temperature shown in Fig. 3 can also be explained by the above model, i.e., a larger W^* for release of the quenched strain in Fig. 5 indicates that the larger volume of flow unit is the source of the temperature memory effect at a higher SA temperature. In such a case, a larger quenched elastic strain can be expected as illustrated in Figs. 6(e)–6(g). From the activation energy difference, the volume of flow unit for the highest SA temperature is about two times larger than those of the lowest SA temperature. If the number of flow units of each size in the ribbon is about the same, the difference in quenching strain for each ribbon may follow the same trend. The observed difference is about a factor of 3, which may indicate that the number of larger flow units increases moderately with increasing SA temperature.

Hilzinger *et al.* have pointed out that SA induced magnetic anisotropy is both erasable and rewritable at least twice for $Co_{66}Fe_4Mo_2Si_{16}B_{12}$ [26]. The result indicates that the cage structure is stable, for least a four times exposure to

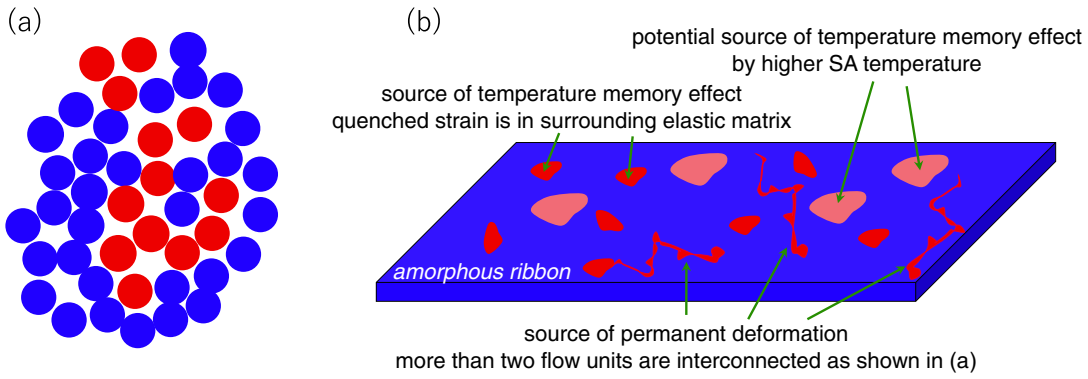

FIG. 7. Overall view of the ribbon during SA. (a) The region starts to interconnect to adjacent flow units and it becomes a source of permanent deformation. Panel (b) represents the ribbon at a medium SA temperature at which the small flow unit starts to interconnect and the atoms in the bigger flow unit (shown in light red color) have not achieved high mobility. Only those units which have the proper size (isolated and shown in a deep red color) have enough mobility and accommodate to the elongated cage without changing the number density of atoms inside the cage. As a result, the elastic matrix surrounding the red flow unit has quenched strain. They are the source of temperature memory effect at medium SA temperatures.

400 °C. In contrast, permanent elongation always associates with the SA process. Compositional and temperature dependence of permanent elongation up to 3% has been reported by Fernandez-Gubieda *et al.* [28] together with SA induced magnetic anisotropy. In our experiments, the permanent elongations are in the range of 3–5% depending on the SA temperatures, which suggests that some of the cage structures are already breaking down at the SA temperatures. Wang *et al.* proposed that the flow units link with adjacent ones for a higher temperature of the β relaxation [11], as shown in Fig. 7(a). Nevertheless, all SA ribbons show a temperature memory effect which indicates the existence of stable cages. These results suggest that a wide size distribution of the flow units and the occurrence of the breaking down of cages smaller than those contributing to the temperature memory effect is the source for the permanent deformation shown in Fig. 7(b). The recent molecular dynamics simulations show the stringlike atomic motion corresponding to β relaxation [17]. Interestingly, the simulation shows both the linearlike and aggregated geometry which are similar to the permanent deformation and temperature memory regions in our model, respectively. A broad size distribution of flow units is also deduced from the wide range of the observed temperature memory effect and the dependence of the activation energy on the SA temperatures. This could be the reason why no indication of β relaxation appears in calorimetry measurements, i.e., the signal is stretched into the wide temperature range compared to a metallic glass which shows a clear signal of β relaxation. However, the temperature memory effect strongly indicates the same structural feature here as with the bulk metallic glasses with $T_g < T_x$, i.e., the existence of a localized flow unit (β relaxation region) surrounded by an elastic matrix.

Evaluating the values of the flow unit volume using Eq. (2) may be useful for comparison to metallic glasses with $T_g < T_x$. Following the previous studies [10,36,37], $\gamma_c \sim 0.027$ and $\xi \sim 3$ are used for the configuration parameters, and the Young's modulus $E = 17.4 \times 10^{10}\,\mathrm{N/m^2}$ (174 GPa) for $Co_{75}Si_{10}B_{15}$ [38]. The Poisson ratio ν is taken as from 0.3 to 0.4, which is the typical range for bulk metallic glasses [10,39,40] and the relation between E and the shear modulus G, $G = E/[2(1+\upsilon)]$, yields values of 62–67 GPa for G. Putting those values into Eq. (2), the value of Ω falls in the range from 1.3 to 1.5 $\mathrm{nm^3}$ for the sample annealed at 280 °C, and 2.6 to 2.8 $\mathrm{nm^3}$ for the sample annealed at 400 °C as rough evaluations of the flow unit volume. Those values are relatively small compared to those reported for metallic glass systems with $T_g < T_x$, which are mostly in the range of 3–6 $\mathrm{nm^3}$. Smaller Ω and a wide size distribution may be the characteristic difference between glasses with $T_g < T_x$ and those with $T_g > T_x$. To confirm this, further studies and simulations will be required.

V. CONCLUSIONS

By employing SA, elastic strain can be quenched in $Co_{72.5}Fe_{1.5}Mn_4Si_5B_{17}$ metallic glass ribbons. The subsequent annealing causes the release of the quenched strain. The maximum rate of the strain release is observed at about the same temperature used for the SA, therefore, a "temperature memory effect" is confirmed. The origin of the temperature memory effect can be well explained by the the localized flow unit which is the source of β relaxation and is used as the model for shear band formation and rejuvenation in the metallic glasses with $T_g < T_x$. Different activation energies for releasing strain were observed depending on the SA temperatures, indicating a wide distribution of flow unit volumes. Since quenching of elastic strain is the origin of the SA-induced magnetic anisotropy known in many Fe, Ni, and Co based amorphous ribbons, the same structure must be generally present in all of them. The results clearly indicate that the nature of ferromagnetic ribbons with $T_g > T_x$ are on the same lines as recently studied metallic glasses with $T_g < T_x$. Therefore, in addition to the ferromagnetic ribbons, the temperature memory effect may appear in bulk metallic glasses under certain SA conditions. Since the elastic strain is very sensitive in magnetization behavior, detailed studies will hopefully revive interest in ferromagnetic metallic glass ribbons and prove to be a great help in understanding more

about the nature of the localized flow unit as well as nonaffine deformations.

ACKNOWLEDGMENT

This work was partially supported by KAKENHI Grant No. JSPS-15K06418.

P.K., M.O., and G.H. contributed to writing the paper. M.O. led the project and made the model. Preparation of amorphous ribbons and stress annealing was by M.K., M.O., C.P., and G.H. The XRD and LTE measurements and their analysis were by P.K., R.H., and K.T.

[1] G. Herzer, M. Vazquez, M. Knobel, A. Zhukov, T. Reininger, H. Davies, R. Groessinger, and J. S. Ll, Round table discussion: Present and future applications of nanocrystalline magnetic materials, J. Magn. Magn. Mater. **294**, 252 (2005).

[2] R. C. O'Handley, Magnetic materials for EAS sensors, J. Mater. Eng. Perf. **2**, 211 (1993).

[3] R. Hasegawa, Advances in amorphous and nanocrystalline magnetic materials, J. Magn. Magn. Mater. **304**, 187 (2006).

[4] M. Malatek and L. Kraus, Off-diagonal GMI sensor with stress-annealed amorphous ribbon, Sens. Actuators A **164**, 41 (2010).

[5] G. Herzer, Modern soft magnets: amorphous and nanocrystalline materials, Acta Mater. **61**, 718 (2013).

[6] A. Inoue, Stabilization of metallic supercooled liquid and bulk amorphous alloys, Acta Mater. **48**, 279 (2000).

[7] F. Spaepen, A microscopic mechanism for steady state inhomogeneous flow in metallic glasses, Acta Metall. **25**, 407 (1977).

[8] J. C. Ye, J. Lu, C. T. Liu, Q. Wang, and Y. Yang, Atomistic free volume zones and inelastic deformation of metallic glasses, Nat. Mater. **9**, 619 (2010).

[9] H. Wagner, D. Bedorf, S. Küchemann, M. Schwabe, B. Zhang, W. Arnold, and K. Samwer, Local elastic properties of a metallic glass, Nat. Mater. **10**, 439 (2011).

[10] S. T. Liu, Z. Wang, H. L. Peng, H. B. Yu, and W. H. Wang, The activation energy and volume of flow units of metallic glasses, Scr. Mater. **67**, 9 (2012).

[11] Z. Wang, B. A. Sun, H. Y. Bai, and W. H. Wang, Evolution of hidden localized flow during glass-to-liquid transition in metallic glass, Nat. Commun. **5**, 5823 (2014).

[12] J. Ding, S. Patinet, M. L. Falk, Y. Cheng, and E. Ma, Soft spots and their structural signature in a metallic glass, PNAS **111**, 14052 (2014).

[13] F. Meng, K. Tsuchiya, S. Ii, and Y. Yokoyama, Reversible transition of deformation mode by structural rejuvenation and relaxation in bulk metallic glass, Appl. Phys. Lett. **101**, 121914 (2012).

[14] S. V. Ketov, Y. H. Sun, S. Nachum, Z. Lu, A. Checchi, A. R. Beraldin, H. Y. Bai, W. H. Wang, D. V. Louzguine-Luzgin, M. A. Carpenter, and A. L. Greer, Rejuvenation of metallic glass by non-affine thermal strain, Nature (London) **524**, 200 (2012).

[15] M. Wakeda and J. Saida, Heterogeneous structural changes correlated to local atomic order in thermal rejuvenation process of Cu-Zr metallic glass, Sci. Technol. Adv. Mater. **20**, 632 (2019).

[16] T. Ichitsubo, E. Matsubara, T. Yamamoto, H. S. Chen, N. Nishiyama, J. Saida, and K. Anazawa, Microstructure of Fragile Metallic Glasses Inferred from Ultrasound-Accelerated Crystallization in Pd-Based Metallic Glasses, Phys. Rev. Lett. **95**, 245501 (2005).

[17] H. B. Yu, R. Richert, and K. Samwer, Structural rearrangements governing johari-goldstein relaxation in metallic glasses, Sci. Adv. **3**, e1701577 (2017).

[18] Y. Tong, W. Dmowski, Z. Witczak, C-P. Chuang, and T. Egami, Residual elastic strain induced by equal channel angular pressing on bulk metallic glasses, Acta Mater. **61**, 1204 (2013).

[19] H. Fujimori, T. Masumoto, Y. Obi, and M. Kikuchi, On the magnetization process in an iron-phosphorus-carbon amorphous ferromagnet, Jpn. J. Appl. Phys. **13**, 1889 (1974).

[20] F. E. Luborsky, J. J. Becker, and R. O. McCary, Magnetic annealing of amorphous alloys, IEEE Trans. Magn. **11**, 1644 (1975).

[21] R. S. Williams and T. Egami, Effect of deformation and annealing on magnetic amorphous alloys, IEEE Trans. Magn. **12**, 927 (1976).

[22] F. E. Luborsky, J. L. Walter, and D. G. LeGrand, Cold rolling and annealing of amorphous ribbons, IEEE Trans. Magn. **12**, 930 (1976).

[23] T. Egami, P. J. Flanders, and C. D. Graham Jr., Low field magnetic properties of ferromagnetic amorphous alloys, Appl. Phys. Lett. **26**, 128 (1975).

[24] F. E. Luborsky and J. J. Becker, Strain-induced anisotropy in amorphous alloys and the effect of toroid diameter on magnetic properties, IEEE Trans. Magn. **15**, 1939 (1979).

[25] O. V. Nielsen and H. J. V. Nielsen, Strain- and field-induced magnetic anisotropy in metallic glasses with positive or negative λs, Solid State Commun. **35**, 281 (1980).

[26] H. R. Hilzinger, Stress induced magnetic anisotropy in an non-magnetostrictive amorphous alloy, in *Proceedings of the 4th International Conference on Rapidly Quenched Metals* (Japan Institute of Metals, Sendai, Japan, 1981), p. 791.

[27] O. V. Nielsen, Separation into two contributions of stress anneal induced magnetic anisotropy in metallic glass ribbons, J. Magn. Magn. Mater. **36**, 81 (1983).

[28] M. L. Fernandez-Gubieda, J. M. Barandiaran, and O. V. Nielsen, Simultaneous observation of viscoelastic deformation and induced magnetic anisotropy in $[Co_{1-x}(FeNi)_x]_{75}Si_{15}B_{10}$ metallic glasses, J. Appl. Phys. **62**, 2579 (1987).

[29] G. Herzer and R. Schulz, United States Patent, No. 6254695 (2001).

[30] W. Dmowski and T. Egami, Observation of structural anisotropy in metallic glasses induced by mechanical deformation, J. Mater. Res. **22**, 412 (2007).

[31] A. Jurikova, K. Csach, J. Miskuf, and V. Ocelik, Creep recovery of metallic glass Fe-Ni-B after longtime stress annealing, Czechoslovak J. Phys. **54**, 129 (2004).

[32] M. Ohnuma, G. Herzer, P. Kozikowski, C. Polak, V. Budinsky, and S. Koppoju, Structural anisotropy of amorphous alloys with creep-induced magnetic anisotropy, Acta Mater. **60**, 1278 (2012).

[33] P. Kozikowski, M. Ohnuma, G. Herzer, C. Polak, V. Budinsky, S. Koppoju, M. Lewandowska, and K. J. Kurzydlowski, Relaxation studies of amorphous alloys with creep induced magnetic and structural anisotropy, Scr. Mater. **67**, 763 (2012).

[34] G. Herzer, S. Flohrer, and C. Polak, Effect of stress annealing on the saturation magnetostriction of nanocrystalline $Fe_{73.5}Cu_1Nb_3Si_{15.5}B_7$, IEEE Trans. Magn. **46**, 341 (2010).

[35] M. Gao and J. H. Perepezko, Separating β relaxation from α relaxation in fragile metallic glasses based on ultrafast flash differential scanning calorimetry, Phys. Rev. Mater. **4**, 025602 (2020).

[36] W. L. Johnson and K. Samwer, A University Criterion for Plastic Yielding of Metallic Glass with a $(T/T_g)^{2/3}$ Temperature Dependence, Phys. Rev. Lett. **95**, 195501 (2005).

[37] J. S. Harmon, M. D. Demetrious and W. L. Johnson, and K. Samwar, Anelastic to Plastic Transition in Metallic Glass-Forming Liquid, Phys. Rev. Lett. **99**, 135502 (2007).

[38] A. Inoue, H. S. Chen, J. T. Krause, T. Masumoto, and M. Hagiwara, Young's modulus of Fe-, Co-, Pd- and Pt-based amorphous wires produced by the in-rotating water spinning method, J. Mater. Sci. **18**, 2743 (1983).

[39] C. P. Chou, L. A. Davis, and M. C. Narasimhan, Elastic constants of metallic glasses, Scr. Metall. **11**, 417 (1977).

[40] Z. Long, Y. Shao, G. Xie, P. Zhang, B. Shen, and A. Inoue, Enhanced soft-magnetic and corrosion properties of Fe-based bulk glassy alloys with improved plasticity through the addition of Cr, J. Alloys Compd. **462**, 52 (2008).